Seismic data reconstruction of primaries and multiples

Francisco Miranda
University of Houston

Abstract

Seismic data reconstruction is an important practical prerequisite for the most complete "full wavefield" seismic processing algorithms (e.g., in multiple attenuation and imaging) that expect areal coverage on the measurement surface. Our objectives are to 1.) develop a clear and complete conceptual framework for data reconstruction of the entire wavefield at the measurement surface, that includes all seismic events (primaries and multiples), and 2.) develop practical algorithms for interpolation and extrapolation that adhere to this framework.

The most sophisticated data reconstruction techniques combine an inverse step followed by a forward data generation step. We show that the combination of making the inverse Born approximation followed by a forward Born-like data generation is applicable to both primaries and multiples, despite the single-scattering assumption of both the forward and inverse Born approximations.

We analyze an aperture-limited migration algorithm with constant background velocity for a 1D earth and study the ability to interpolate and extrapolate with different starting apertures in the pre-critical and post-critical zones. Data reconstruction with multiples is also tested, and the implications for free surface multiple removal are considered. We conclude that, with our approach, we can effectively reconstruct seismic data in the pre-critical region using data recorded at pre-critical offsets. Extrapolating from post-critical to pre-critical offsets confronts us with phase problems due to the reflectivity in the post-critical region. We show, for a simple example, that both primary and multiple reflections are reconstructed accurately in both time and amplitude.

1 Introduction and motivation

The search for hydrocarbons in ever more complex geological areas calls for more advanced seismic processing algorithms that make fewer and less rigid assumptions about *a priori* information relating to the subsurface (Weglein et al., 2003). These algorithms invariably require that seismic data be adequately sampled on the acquisition surface (in both the inline and crossline directions). The demands of these methods motivates research into new procedures for data interpolation and extrapolation.

One of the most challenging problems in marine exploration is incomplete data coverage. In particular the problem of missing data in the cross-line direction perpendicular to the

streamers is an impediment to effective removal of multiples and depth imaging of the data. For example, wave-theoretic multiple attenuation algorithms, such as the demultiple algorithms derived by Weglein et al. (1997) from the inverse scattering series, and other methods (e.g., Verschuur et al., 1992) are applicable to an unknown 3-D earth but expect data sampled on a grid at the surface to effectively attenuate all multiples. Extrapolation of near offsets is another important prerequisite for multiple attenuation and can be particularly challenging in shallow water where the first receiver records data in the post-critical regime. Wave-theoretic depth imaging algorithms (e.g., Claerbout, 1971; Stolt, 1978) also expect more complete data coverage than is typically acquired.

Although recent progress has been reported on the application of 3D free surface demultiple through a combination of acquisition and data reconstruction, it is recognized that the success of the combination critically depends on the effectiveness of the data extrapolation, and that is an area that could benefit from increased efficacy.

Different mapping operators have been developed, some simple and some complex, depending on their underlying assumptions and approximations. In general, the mapping operators can be classified into two groups: 1.) full seismic data reconstruction where the reflectivity depends on the incident angle (e.g., Stolt, 2002); and 2.) basic mapping reconstruction algorithms that are independent of incident angle.

In seismic data reconstruction, there are different components to be addressed. The fundamental idea of the proposed theory is a consecutive application of a Born-approximated migration, and demigration. The key elements of this approach are a weighted Kirchhoff-type diffraction stack performed for depth migration using the inverse Born approximation, and a weighted Kirchhoff-type isochron stack integral for demigration using the forward Born approximation (Hubral et al., 1996; Santos et al., 2000). Although there are substantial differences between the inverse and the forward Born approximation, a combination of the two yields positive results regarding the seismic data reconstruction process. This is explained in the following section.

2 Forward and inverse scattering; A framework for data reconstruction

Forward scattering constructs the seismic wavefield, D, at any point in terms of reference medium propagation while inverse scattering inverts seismic data in terms of reference propagation. The forward scattering series is given by

$$D = G_0 V G_0 + G_0 V G_0 V G_0 + \cdots \tag{1}$$

where G_0 is the impulse response due to a point source in the reference medium and V is the perturbation operator, which is the difference between the linear differential operators that describe wave propagation in the reference model and the actual model (L_0 and L,

respectively). Events in time are difficult to predict in the forward series since the wave is propagating with the reference velocity. It takes an infinite sum to predict events at the correct time using the forward series. However, the forward series is an exact equation for primaries and multiples when it converges.

A widely-used approximation for inverting seismic data stems from the the assumption that, when V is small in some sense, then the truncation of the series for the first term leads to

$$D \approx G_0 V G_0. \tag{2}$$

This expression is the forward Born approximation and is not a good estimate for either primaries or multiples. It gives the incorrect time and a poor approximation to the amplitude of events.

To derive the inverse series, we consider the perturbation V as an expansion

$$V = \sum_{n=1}^{\infty} V_n = V_1 + V_2 + V_3 + \cdots \tag{3}$$

where V_1 is the linear approximation to the earth properties. The inverse series is an infinite series in orders of the data on the measurement surface, D_0 (Weglein et al., 2003).

$$D_0 = \Lambda_g \sum_{n=1}^{\infty} (G_0 V)^n G_0 \Lambda_s = \Lambda_g (G_0 V G_0 + G_0 V G_0 V G_0 + \cdots) \Lambda_s \tag{4}$$

where Λ_g and Λ_s are the projection of the field to the measurement surface. Introducing the parameter ϵ in (3), we will have $V = \sum \epsilon^n V_n$, and because we are on the measurement surface $D_0 \Rightarrow \epsilon D_0$.

$$\epsilon D_0 = \Lambda_g (G_0 \epsilon V_1 G_0 + G_0 \epsilon^2 V_2 G_0 + \cdots + G_0 \epsilon V_1 G_0 \epsilon V_1 G_0) \Lambda_s. \tag{5}$$

The first order term is identified with ϵ of first order

$$\epsilon^1 : D_0 = \Lambda_g G_0 V_1 G_0 \Lambda_s. \tag{6}$$

The second order terms contain ϵ^2 coefficients

$$\epsilon^2 : 0 = \Lambda_g G_0 V_2 G_0 \Lambda_s + \Lambda_g G_0 V_1 G_0 V_1 G_0 \Lambda_s \tag{7}$$

and the nth order terms contain ϵ^n coefficients

$$\epsilon^n : 0 = \Lambda_g G_0 V_n G_0 \Lambda_s + \Lambda_g G_0 V_1 G_0 V_{n-1} G_0 \Lambda_s + \cdots + \Lambda_g G_0 V_1 G_0 V_1 G_0 \cdots G_0 V_1 G_0 \Lambda_s. \tag{8}$$

Equations (6)–(8) are the inverse scattering series and the same original reference operator G_0 is inverted at each step to solve for V_n. The inverse Born approximation is defined by

$$\epsilon^1 : D_0 \approx \Lambda_g G_0 V G_0 \Lambda_s. \tag{9}$$

As shown, V_1 is the portion of V that is linear in the data.

The inverse series starts with data in time, hence it favors tasks with the reference velocity. By the nature of its terms, it has all the ingredients to work as an extrapolator, and its benefits are shown in the next section. From our understanding of the forward series, we might consider the first term in the inverse series as single scattering process, but the inverse series is a series in the data and this interpretation may cause some confusion.

Mathematically, the difference between the inverse Born approximation (9) and the forward Born approximation (2) is the substitution of V_1 in the first case, and V in the second. The expression (9) is not only good for primaries and multiples, it is exact and precise without a thought or care about convergence. This understanding is at the heart of the first step of the inverse series as well as the engine for extrapolation. The success of seismic data reconstruction for multiples is based on the combination of inverse and forward. In some sense the demigration is the inverse task to migration, and by this rule it can handle multiples.

3 Aperture Migration, a 1D Example

3.1 Finite aperture migration

To invert for medium properties requires choosing the set of parameters that you want to invert for. The chosen set of parameters defines an earth model type, and the details of the data reconstruction will depend on that choice. The meaning of a model-type-independent task-specific subseries is that the defined task is achievable with precisely the same algorithm for an entire class of earth model types. From this consideration we conclude that seismic data reconstruction is model type dependent.

We start with a convenient reflection model, realistic at moderate reflection angles provided by perturbation theory. This model assumes that the reflections are caused by small and rapid deviations from a constant background. In this model every subsurface point can reflect seismic energy.

Under this assumption, we also assume that we are dealing with a pressure field described by the scalar wave equation. G_0 is the unit impulse response in a background of homogeneous velocity c, and G is the unit impulse response for the actual inhomogeneous velocity v. Thus G and G_0 obey the scalar wave equations

$$\left(\nabla^2 - \frac{1}{v^2}\frac{\partial^2}{\partial t^2}\right) G = -\delta(t_g - t_s)\delta(x_g - x_s)\delta(z_g - z_s) \ , \ \ G = 0 \ \ \ t < 0 \tag{10}$$

and

$$\left(\nabla^2 - \frac{1}{c^2}\frac{\partial^2}{\partial t^2}\right) G_0 = -\delta(t_g - t_s)\delta(x_g - x_s)\delta(z_g - z_s) \ , \ \ G_0 = 0 \ \ \ t < 0 \tag{11}$$

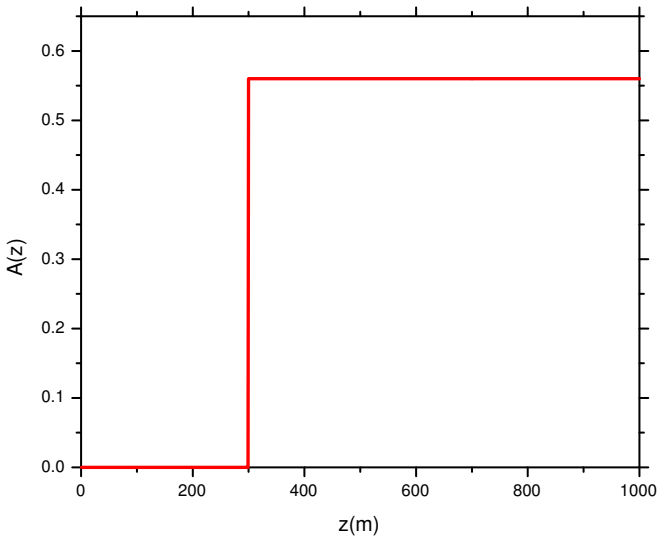

Figure 1*: An acoustic 1D earth model with two medium velocities. The first medium has* $c = 1500$ *m/s and the second medium with* $v = 2250$ *m/s.*

Here (x_g, z_g) and (x_s, z_s) are source and receiver locations respectively. $t = t_g - t_s$ is the travel time from source to receiver. By subtracting (10) from (11) we obtain

$$\left(\nabla^2 - \frac{1}{c^2}\frac{\partial^2}{\partial t^2}\right)(G - G_0) = -\left(\frac{1}{c^2} - \frac{1}{v^2}\right)\frac{\partial^2}{\partial t^2}G. \tag{12}$$

Defining the difference between impulse responses, $P = G - G_0$, as the scattered wavefield, the solution for P can be expressed as an integral equation

$$\begin{aligned} P(x_g, z_g|x_s, z_s; t_s - t_g) &= \int dx \int dz \int dt\, G_0(x_g, z_g|x, z; t_g - t) \\ &\quad \frac{A(z)}{c^2}\frac{\partial^2}{\partial t^2}G(x, z|x_s, z_s; t - t_s). \end{aligned} \tag{13}$$

where $A(z)$, shown in Figure 1, is the velocity perturbation and is defined as

$$A(z) = 1 - \frac{c^2}{v^2} \tag{14}$$

c is the velocity in the background medium and v is the true velocity of our model. Here there is a combination of the transmission term G_0 which carries energy from source to reflector, the reflector response A, and the transmission term G that carries energy from the reflector to the surface. G is the perturbed field, and it contains the direct wave and all

multiple reflections. To linearize this equation, G is replaced by G_0 using the first two terms of the Born series obtained from the Lippmann-Schwinger equation

$$\begin{aligned} P(x_g, z_g|x_s, z_s; t_s - t_g) &= \int dz \int dx \int dt\, G_0(x_g, z_g|x, z; t_g - t) \\ &\quad \times \frac{A(z)}{c^2} \frac{\partial^2}{\partial t^2} G_0(x, z|x_s, z_s; t - t_s)\ . \end{aligned} \tag{15}$$

Equation (15) corresponds to the Born approximation in (2). Physically the approximation of G by G_0 means that all but primary reflections are neglected.

The solution to equation (11) in the frequency domain is given by

$$G_0(k_{gx}, k_{gz}|z; \omega, t_g) = -e^{i(\omega t_g - k_{gx} x)} \frac{e^{-ik_{gz}|z_g - z|}}{2ik_{gz}} \tag{16}$$

$$G_0(k_{sx}, k_{sz}|x_s, z_s; \omega, t_s) = -e^{i(\omega t_s - k_{sx} x)} \frac{e^{-ik_{sz}|z - z_s|}}{2ik_{sz}} \tag{17}$$

where

$$k_{gz} + k_{sz} = sgn(\omega)\sqrt{\frac{\omega^2}{c^2} + k_{gx}^2} + sgn(\omega)\sqrt{\frac{\omega^2}{c^2} + k_{sx}^2} \tag{18}$$

Equation (15) becomes

$$P(k_{gx}, 0|k_{sx}, 0; \omega) = -\int dx \int dz \frac{e^{-ik_{gz}|z|}}{2ik_{gz}} e^{-i(k_{gx} x)} A(z) \frac{\omega^2}{c^2} \frac{e^{-ik_{sz}|z|}}{2ik_{sz}} e^{i(k_{sx} x)} \tag{19}$$

$$= 2\pi \frac{\omega^2}{c^2} \frac{A(k_z)}{k_z^2} \tag{20}$$

where $k_z = k_{gz} + k_{sz}$. There are different ways to invert equation (20). We exploit the degree of freedom to compensate the aperture to a finite region by using a weight function $L(k_z, k_{gx})$. It must carry the information of the aperture and satisfy the constraint

$$\int \frac{\omega^2}{k_z^2} \cdot 2\pi \cdot L(k_{gx}, k_z) \cdot dk_{gx} = 1. \tag{21}$$

The migrated image is then described by

$$A(z) = \frac{1}{2\pi} \int e^{-ik_z \cdot z} \cdot dk_z \int L(k_{gx}, k_z) \cdot dk_{gx} \int dx_g \cdot e^{-ik_{gx} \cdot x_g} \cdot P(x_g, c \cdot \sqrt{k_z^2/4 + k_{gx}^2}). \tag{22}$$

In other words

$$A(z) = \int dx_g \int d\omega \cdot I(z, x_g, \omega) \cdot P(x_g, \omega) \tag{23}$$

where

$$I(z, x_g, \omega) = \frac{1}{2\pi} \int_{-\infty}^{\infty} \frac{\omega}{c} L\left(\frac{\omega}{c}\xi,\ 2\frac{\omega}{c}\sqrt{1 - \xi^2}\right) e^{-\frac{\omega}{c}(2\sqrt{1-\xi^2} \cdot z + \xi \cdot x_g)} \frac{2}{c\sqrt{1 - \xi^2}} d\xi \tag{24}$$

and

$$\xi = \frac{c}{\omega} k_{gx}. \tag{25}$$

In general, the integral (24) cannot be solved analytically. However, it may be simplified to an approximate ray-theoretical expression via the method of stationary phase, which provides a way of analyzing the main contributions. Reducing it to its basic structure, the integral in equation (24) can be written in the form

$$I(\omega) = \int_{-\infty}^{\infty} f(\xi) \cdot e^{i\omega q(\xi)} d\xi. \tag{26}$$

The method of stationary phase is based on the observation that for high frequencies, the factor $e^{i\omega q(\xi)}$ oscillates very rapidly, thus covering full periods in very small intervals of ξ, (for details, see appendix A).

If $f(\xi)$ is not itself an oscillating function, its values do not strongly vary in any such interval. Thus, the integration over a full period of $e^{i\omega q(\xi)}$ yields approximately zero and does not contribute to the overall value of the integral. The only regions where it does not oscillate are those where the phase function $q(\xi)$ remains approximately constant or stationary.

For aperture migration, the limits of integrations of expression (26) are going to change to finite values a and b, because of finite data consideration, reducing to the integral

$$I(\omega) = \int_{a}^{b} f(\xi) \cdot e^{i\omega q(\xi)} d\xi. \tag{27}$$

The analysis of the migration integral by the stationary phase approximation yields

$$I(\omega) \simeq f(\xi_{st}) e^{i\omega q(\xi_{st})} \sqrt{\frac{2\pi}{-\omega q"(\xi_{st})}} + \frac{1}{i\omega} \left[\frac{f(b)}{q'(b)} e^{i\omega q(b)} - \frac{f(a)}{q'(a)} e^{i\omega q(a)} \right] \tag{28}$$

where ξ_{st} is the stationary point of the phase $q = \tau_D - \tau_R$, that is the tangency point between the Huygens and the reflection traveltime curves. The first term of the expression (28) is the dominant part of the total migrated section, and the second terms comes from the endpoints of the integration/stacking operator.

3.2 Regularization by neutralizers

Using separation of variables, the aperture compensation function is described as the product of two functions: the first one carries geometrical information about the aperture and the second carries information about the phase (Stolt and Benson, 1986)

$$L(k_x, k_z) = S\left(\frac{k_{gx}}{k_z}\right) \cdot F(c \cdot \sqrt{k_z^2/4 + k_{gx}^2}). \tag{29}$$

According to Bleistein and Handelsman (1986), a neutralizer is defined to be one if it is in the neighborhood of a stationary value and zero outside this region. For a regularization with a neutralizer function, we have

$$S\left(\frac{k_{gx}}{k_z}\right) = B(h_1, h_2, x_g - x_s) \cdot T(k_{gx}/k_z) \tag{30}$$

where $T\left(k_{gx}/k_z\right)$ is a weight function that compensates for the amplitude and $B(h_1, h_2)$ is our neutralizer function defined (in the limits of the aperture, with h_1 as the starting aperture offset and h_2 final aperture offset) as

$$B(h_1, h_2, x_g - x_s) = \begin{cases} 1 & (x_g - x_s) \in (h_1, h_2) \\ 0 & \text{otherwise} \end{cases} \tag{31}$$

Defining $\beta = k_{gx}/k_z$, $\gamma = ck_z/2$ and the evaluation of the end points of the aperture $\beta_1 = k_{xstat}/k_{zstat} = x_{g1}/4z$ $\beta_2 = k_{xstat}/k_{zstat} = x_{g2}/4z$ we can express (21) as

$$\int_{\beta_1}^{\beta_2} S(\beta) \cdot F(\gamma \cdot \sqrt{1+4\beta^2}) \cdot \frac{1/c^2 \cdot \gamma^2 \cdot (1+4\beta^2)}{4\gamma^2/c^2} \cdot 2\pi \cdot \frac{d\beta}{2\gamma/c} = 1 \tag{32}$$

where F is an arbitrary function to be chosen. If we choose $F(\gamma \cdot \sqrt{1+4\beta^2}) = \gamma \cdot \sqrt{1+4\beta^2}/c$, then (21) becomes

$$\int S(\beta) \cdot (1+4\beta^2)^{3/2} \cdot \frac{\pi}{4} \cdot d\beta = 1. \tag{33}$$

Finally, the expression for aperture compensation using a neutralizer is defined as

$$L(k_{gx}, k_z) = \frac{c}{\pi} \cdot \frac{\omega^{-1}}{(1+4k_{gx}^2/k_z^2)^{1/2}} \cdot \frac{1}{(\beta_2 - \beta_1)}. \tag{34}$$

3.3 Regularization by taper functions

The neutralizer function can be replaced by a taper function only having partial derivatives up to second order (Sun, 1998, 2002). To be in accordance with the neutralizer function, the taper must be unity within a subaperture and be zero on the boundary of the subaperture, it must decrease smoothly from unity to zero.

Under this assumption,

$$B(h_1, h_2, x_g - x_s) = \frac{1}{2}\left(1 + \cos\left[\pi\left(\frac{\beta - \beta_1}{\beta_2 - \beta_1}\right)\right]\right). \tag{35}$$

According to (35) the aperture compensation function using a taper function is

$$L(k_{gx}, k_z) = \frac{1}{2\pi}\left(1 + \cos\left[\pi\left(\frac{k_{gx}/k_z - \beta_1}{\beta_2 - \beta_1}\right)\right]\right) \frac{\omega^{-1}}{(1+4(k_{gx}/k_z)^2)^{1/2}} \frac{c}{\beta_2 - \beta_1}. \tag{36}$$

For our numerical examples, we use an acoustic earth model that consists of two semi-infinite homogeneous halfspaces. The upper halfspace is defined to have a velocity of $c(z < 300\text{m}) = 1500$ m/s, and the velocity is the lower halfspace is $v(z \geq 300\text{m}) = 2250$ m/s. Density is kept constant over the two halfspaces.

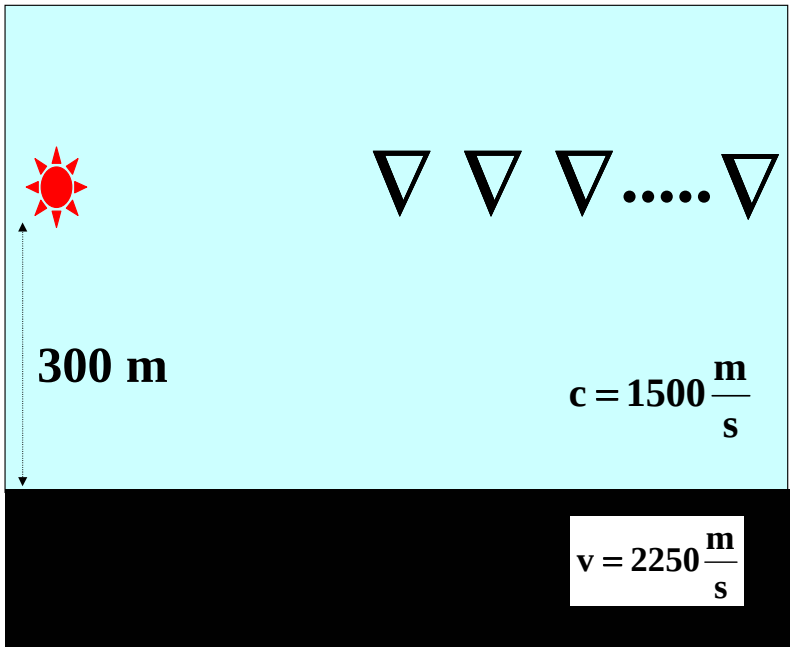

Figure 2: *Model of a single interface. The velocity in the upper and lower media are* $c = 1500$ *m/s and* $v = 2250$ *m/s, respectively, and density is constant.*

4 Structure of the aperture migrated image

The aperture migrated image is given by

$$A(z) = \int dx_g \int d\omega \cdot (I_0 + I_1 + I_2) \cdot P(x_g, \omega) \tag{37}$$

where there is a filtering process, done by the integral over $d\omega$, and also a stacking process, performed by the integral over offset. The three terms in the integrand correspond to contributions from the stationary phase calculation (I_0) and each of the end points of the migration aperture (I_1 and I_2). For a more detailed explanation, see Sun (1998) and Stolt and Benson (1986).

The finite large aperture migration results in a migrated imaged with three parts. One comes from the tangent point between the traveltime curves of the reflected and point-diffracted rays and gives a migrated signal (Jaramillo and Bleistein, 1997). The others are from the

endpoints of the migration aperture and result in migration noise as shown by Hertweck and Goertz (1999).

To guarantee the true-amplitude reconstruction as well as to attenuate migration noise, the migration aperture should be positioned so that its central part contains the tangent point. The true-amplitude weight function should be modified so it tapers the input data near the boundary of the migration aperture.

Depending on where the stationary point is located there are different contributions in the stationary phase form and to the migrated image

$$[-\xi_a, \xi_b] = [-\xi_a, -\xi_c) + (-\xi_c, \xi_c) + (\xi_c, \xi_b]$$

where ξ_a and ξ_b are defined as the evaluation of the stationary point at the end points, and ξ_c is defined as the stationary point inside the aperture.

$$-\xi_a = \frac{x_{g1}}{\sqrt{4z^2 + x_{g1}^2}} \qquad \xi_b = \frac{x_{g2}}{\sqrt{4z^2 + x_{g2}^2}}$$

$$\xi_c = \frac{x_g}{\sqrt{4z^2 + x_g^2}}$$

The migrated image is coming from the evaluation of and the location of the stationary point

$$I = I_{\xi_c} + I_{\xi_a} + I_{\xi_b}. \tag{38}$$

Considering the two-way travel time

$$t = \frac{\sqrt{4z^2 + x_g^2}}{c} \tag{39}$$

also t_{g1} as the evaluation of (39) at $x_g = x_{g1}$, and t_{g2} at $x_g = x_{g2}$.

Depending on where the aperture is located relative to the reflection point we will have, when the stationary point is inside the aperture migration

$$\begin{aligned} A(z) = &\int dx_g \frac{\sqrt{32\pi} z^2}{\pi^2 c^{1/2} \cdot (4z^2 + x_g^2)^{3/4} \cdot (x_{g2} - x_{g1})} \cdot e^{-i\frac{\pi}{4}} \int d\omega \omega^{-1/2} P(x_g, \omega) e^{-i\omega t} \\ &+ \int dx_g \frac{2z^3}{\pi^2 (4z^2 + x_{g2}^2) \cdot (x_{g2} - x_{g1})} \cdot \frac{e^{-i\frac{\pi}{2}}}{(x_g - x_{g_2})} \int d\omega \;\; \omega^{-1} e^{-i\omega\left(t_{g2} + \frac{x_{g2}(x_g - x_{g2})}{c^2 t}\right)} P(x_g, \omega) \\ &- \int dx_g \frac{2z^3}{\pi^2 (4z^2 + x_{g1}^2) \cdot (x_{g2} - x_{g1})} \cdot \frac{e^{-i\frac{\pi}{2}}}{(x_g - x_{g_1})} \int d\omega \omega^{-1} e^{-i\omega\left(t_{g1} + \frac{x_{g1}(x_g - x_{g1})}{c^2 t}\right)} P(x_g, \omega) \end{aligned} \tag{40}$$

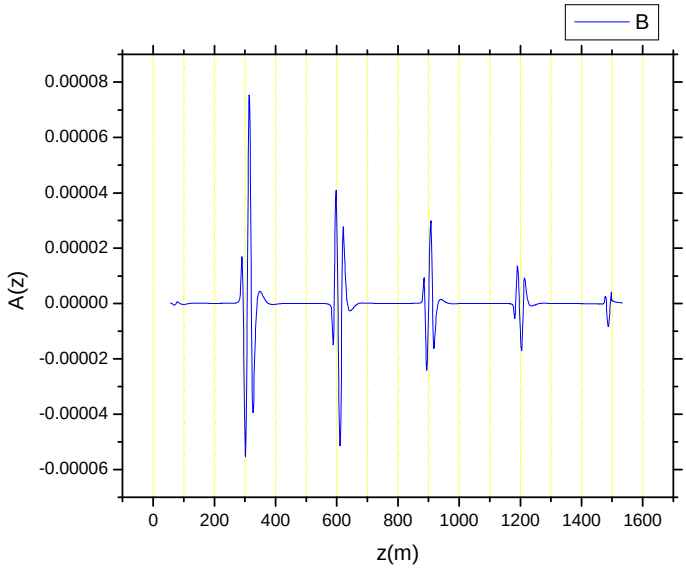

Figure 3*: Migrated image for bandlimited frequency and with the wavelet from the model presented in Figure 2 with a free surface at 15 m above the source and receivers considering that the stationary point is inside the aperture. As it is shown you can see the primary reflection and the free surface multiples.*

The main contribution for the migrated image comes from the first term of the expression above and it is reflected in Figure 3. Figure 3 shows the migrated image of a model similar to the one in Figure 2. The migrated image contains the effect of a free surface located at $z = 0$. The source and receivers are located at 15 m below the free surface. The image is calculated using equation (40), which considers the case where the stationary point is within the acquired offset region.

When the stationary point is outside the acquired offset region,

$$A(z) = \int dx_g \quad \frac{2z^3}{\pi^2(4z^2 + x_{g2}^2) \cdot (x_{g2} - x_{g1})} \cdot \frac{e^{-i\frac{\pi}{2}}}{(x_g - x_{g_2})} \int d\omega\, \omega^{-1} e^{-i\omega\left(t_{g2} + \frac{x_{g2}(x_g - x_{g2})}{c^2 t}\right)} P(x_g, \omega)$$
$$- \int dx_g \frac{2z^3}{\pi^2(4z^2 + x_{g1}^2) \cdot (x_{g2} - x_{g1})} \cdot \frac{e^{-i\frac{\pi}{2}}}{(x_g - x_{g_1})} \int d\omega\, \omega^{-1} e^{-i\omega\left(t_{g1} + \frac{x_{g1}(x_g - x_{g1})}{c^2 t}\right)} P(x_g, \omega) \tag{41}$$

The contribution to the migrated image in this case comes from the end points of the aperture as it is shown in Figure 4. $A(z)$ contains only terms calculated on the edges of the region. The migrated image corresponding to equation (41) is shown in Figure 5. Figure 5 shows

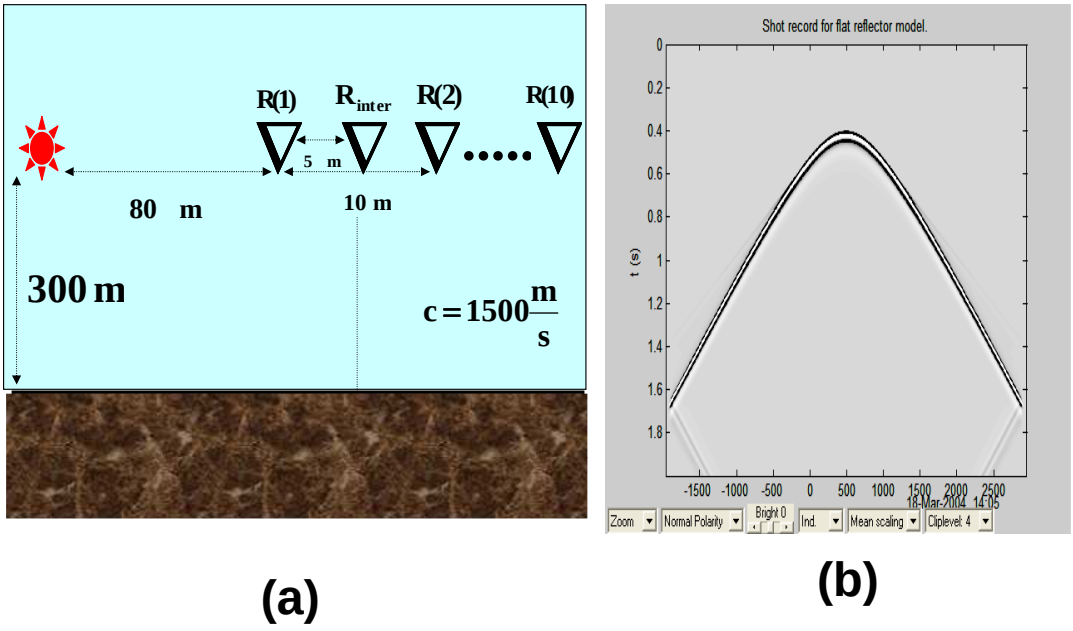

Figure 4: *(a) Schematic representation of the interpolation experiment for a single interface model from pre-critical to pre-critical. (b) Shot record of the model in (a) generated by finite differences.*

a degraded image compared to the one shown in Figure 4 which contains the contribution from a stationary point calculation. Since $A(z)$ deviates from zero between the higher order imaged multiples, we will expect that the data reconstruction of the higher order multiples will be worse than the data reconstruction of the primary and first order multiple.

When the stationary point is at the end point ($\xi_s = \xi_b$),

$$A(z) = \int dx_g \frac{\sqrt{32\pi} z^2}{\pi^2 c^{1/2} \cdot (4z^2 + x_g^2)^{3/4} \cdot (x_{g2} - x_{g1})} \cdot e^{-i\frac{\pi}{4}} \int d\omega \omega^{-1/2} P(x_g, \omega) e^{-i\omega t}$$
$$+ \int dx_g \frac{2z^3}{\pi^2 (4z^2 + x_{g1}^2) \cdot (x_{g2} - x_{g1})} \cdot \frac{e^{-i\frac{\pi}{2}}}{(x_g - x_{g_2})} \int d\omega \omega^{-1} e^{-i\omega \left(t_{g1} + \frac{x_{g1}(x_g - x_{g2})}{c^2 t} \right)} P(x_g, \omega). \tag{42}$$

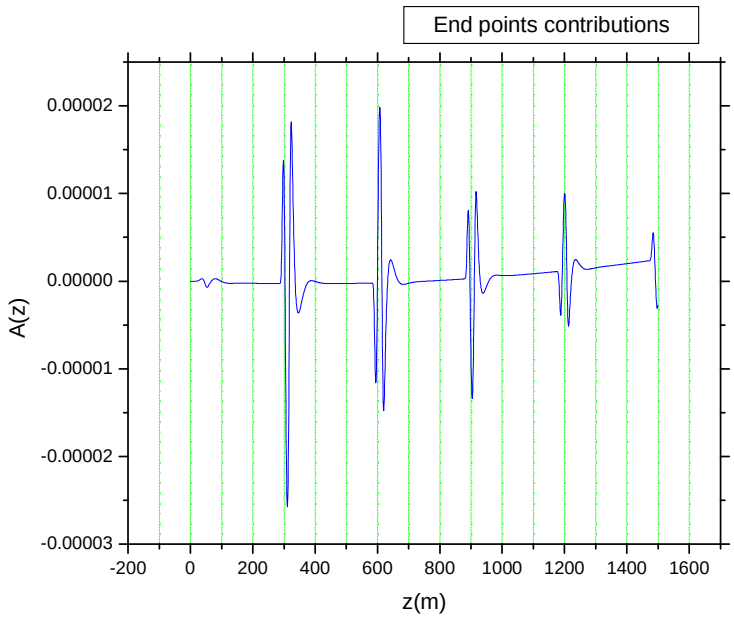

Figure 5*: Migrated image of data from the model shown in Figure 2 but with a free surface at 15 m above the source and receivers. This image is calculated with equation (41) using only the contribution from the end points of the offset range.*

When the stationary point is at the end point($\xi_s = -\xi_a$),

$$A(z) = \int dx_g \frac{\sqrt{32\pi}z^2}{\pi^2 c^{1/2} \cdot (4z^2 + x_g^2)^{3/4} \cdot (x_{g2} - x_{g1})} \cdot e^{-i\frac{\pi}{4}} \int d\omega \omega^{-1/2} P(x_g, \omega) e^{-i\omega t}$$
$$+ \int dx_g \frac{2z^3}{\pi^2 (4z^2 + x_{g1}^2) \cdot (x_{g2} - x_{g1})} \cdot \frac{e^{-i\frac{\pi}{2}}}{(x_g - x_{g_1})} \int d\omega \omega^{-1} e^{-i\omega \left(t_{g1} + \frac{x_{g1}(x_g - x_{g1})}{c^2 t} \right)} P(x_g, \omega). \tag{43}$$

5 Extrapolation procedure

5.1 Data generation: the forward problem

In the previous section, we established a way to calculate an estimate of $A(z)$ based on the acquired finite aperture data. Now we have the means to predict data at each desired location on the acquisition surface. The interpolation/extrapolation procedure (Stolt, 2002) involves using the migrated image as input to the modelling formula in (13) – the forward Born approximation.

It is performed by reintroducing the inversion part $A(z)$ as a function of the data $P(x_g|x_s; t_s - t_g)$ into (13).

$$\begin{aligned} P(x'_g|x_s, t') &= \frac{1}{(2\pi)^3} \int dk'_{gx} \int dk'_{sx} \int d\omega' \, e^{i(k'_{gx}x'_g - k'_{sx}x_s + \omega' t')} \times \\ &\quad \frac{\omega'^2}{4 \cdot \sqrt{\frac{\omega'^2}{c^2} - k'^2_{gx}}} \frac{A(k'_z)}{\sqrt{\frac{\omega'^2}{c^2} - k'^2_{sx}}} \end{aligned} \tag{44}$$

There have been different attempts to solve (44). One approach is to extrapolate the migrated image to new locations by doing a demigration with an approximation in the output. In other words using a stationary phase approximation with respect to k'_{gx} and solving (44)

$$k_{xstat} = + \frac{x'_g k'_z}{2\sqrt{t'^2 c^2 - x'^2_g}} \tag{45}$$

$$P(x'_g|t') = \frac{1}{16\pi} \frac{c^3 t'^2}{\sqrt{2}(x'^2_g - c^2 t'^2)^{5/4}} \int dk'_z e^{-i\left(\frac{\sqrt{t'^2 c^2 - x'^2_g}}{2}\right) k'_z} \sqrt{k'_z} A(k'_z). \tag{46}$$

This approach was presented by Stolt (2002). Using the stationary phase approximation for solving the forward problem, produces a computationally efficient scheme for data reconstruction. In this paper, we deviate from Stolt's approach by calculating the wave field. In this case, calculating the field at each location involves computing contributions from all wavenumbers, k_{gx}.

Changing variables from ω' to k'_z and using the constraint condition (18)

$$P(x'_g|t') = \frac{c}{8\pi} \int dk'_{gx} \int dk'_z \, \frac{e^{i\left(k'_{gx}x'_g - c\, t' \sqrt{\frac{k'^2_z}{4} + k'^2_{gx}}\right)}}{k'_z} \sqrt{\frac{k'^2_z}{4} + k'^2_{gx}} \, A(k'_z). \tag{47}$$

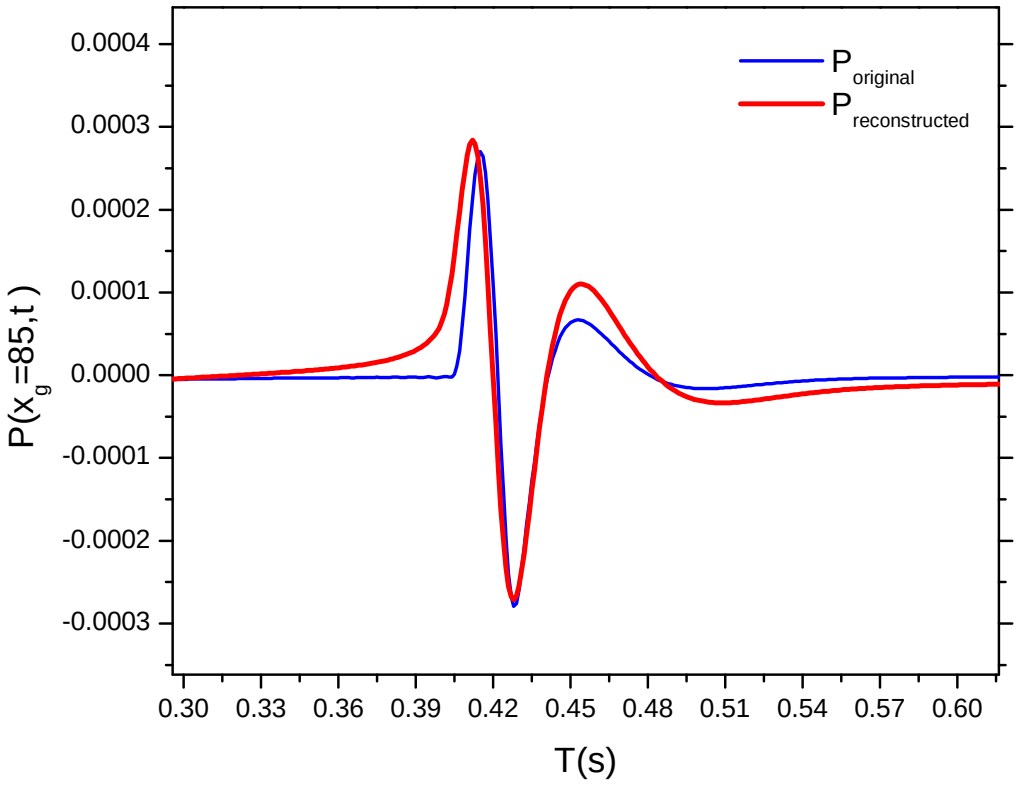

Figure 6*: Interpolated data and the actual data at 85 m from the source when we consider an aperture starting at 70 m until 500 m with a separation of 10 m between receivers.*

5.2 Interpolation in the pre-critical zone

To illustrate the effects of the interpolation/extrapolation schemes, we provide synthetic data examples. We consider the acoustic model defined earlier with a homogeneous half-space of water with one flat reflector at 300 m and no free surface (see Figure 4a). The velocity above the reflector is 1500 m/s and below it is 2250 m/s.

The synthetic shot gather is generated using a finite difference modelling algorithm and using a Ricker wavelet with a center frequency of 30 Hz. The data are sampled at 1 ms, and the record length is two seconds. The shot gather is displayed in Figure 4b.

The algorithm is evaluated on a shot gather where the offset ranges from 70–500 m. The receiver interval is 10 m. We interpolate a trace at an offset of 85 m. Figure 6 shows the results and comparison between the actual modelled data at 85 m and the reconstructed data. The two traces are in good agreement. The interpolated trace appears to be a bit broader than the reference trace.

5.3 Extrapolation from post-critical to pre-critical

We consider a shot gather containing measurements in the offset range 900–1000 m where the receiver spacing is 5 m. The geometry is shown in Figure 7. As shown, the data are measured in the post-critical regime. Our goal is to use the post-critical data for doing inversion and then extrapolate data to the pre-critical zone. An interpolated trace is calculated at offset 475 m and compared with the finite difference modelled trace in Figure 8. There is a considerable phase shift between the two traces. The reason is that the reflection coefficient of the post-critical data is phase-shifted with respect to the pre-critical reflection coefficient. This affects our interpolation results since $A(z)$ is calculated from the post-critical data and will therefore include that phase shift. That phase shift is "propagated" into the new trace when doing the extrapolation.

Several tests have been performed with different apertures beyond the critical angle. The presence of the head wave has an effect on the amplitude. From post-critical to pre-critical data it seems that the reconstructed amplitude increases the accuracy when the presence of the head wave does not mitigate the original signal, as it is shown in Figures 9 and 10. As long as you interpolate or extrapolate to certain limits the procedure is successful. According to this the cascade process of inverse and forward is constrained to the first step.

6 Data reconstruction for data with free surface multiples

As discussed in the introduction, accurate data reconstruction is a practical prerequisite for the most effective multiple attenuation algorithms and must therefore be able to interpolate/extrapolate multiples as well as primaries.

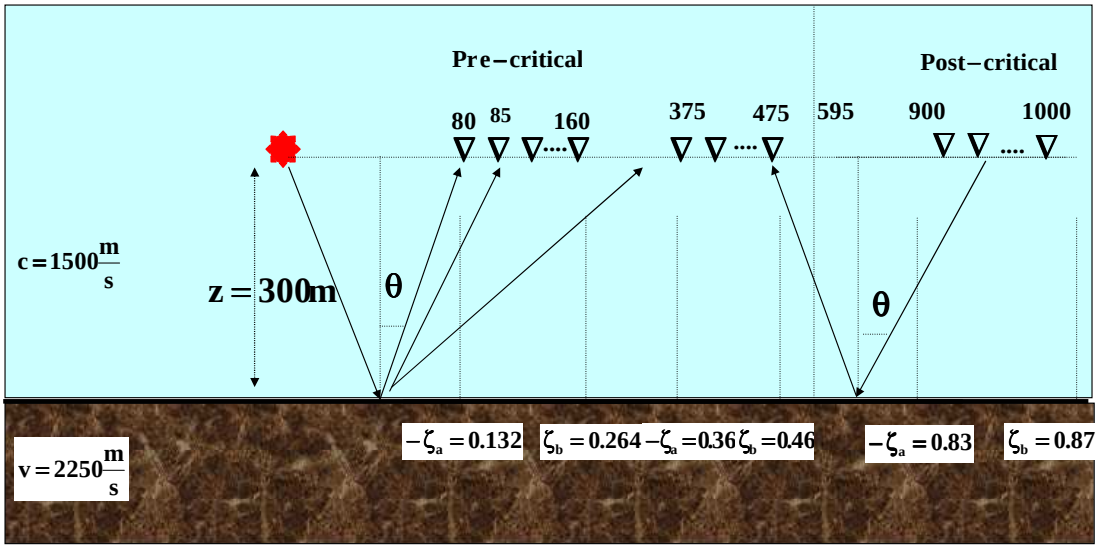

Figure 7*: Schematic representation of the extrapolation experiment for a single interface model from post critical to pre-critical.*

We consider the model described in Figure 11 with a free surface at $z = 0$ m. The source and receivers are located 15 m below the free surface. A finite difference scheme is used to generate the synthetic data and the shot gather is displayed in Figure 11 with the primary at around 0.4 sec. All other events are free surface multiples.

Our goal is to reconstruct data in the near offset region from data acquired in the offset range 150-500 m. The receiver spacing is 5 m. Figure 12 presents the comparison of reconstructed and original data at 100 m from the source. The first event is a primary reflection, which is followed by the first and second order free surface multiples. We note that both the timing and amplitude of the reconstructed data are comparable with the original data. For the objective of multiple prediction, the most important issue is the one of predicted time, and this data reconstruction scheme has calculated the time precisely.

The reconstruction of the primary reflection versus the original one is shown in Figure 13. The amplitude is in the same order of magnitude as the original data, while the time is precisely estimated. The reconstruction of the first order multiple and its original one is shown in Figure 14. Under certain considerations you can always extrapolate data with free

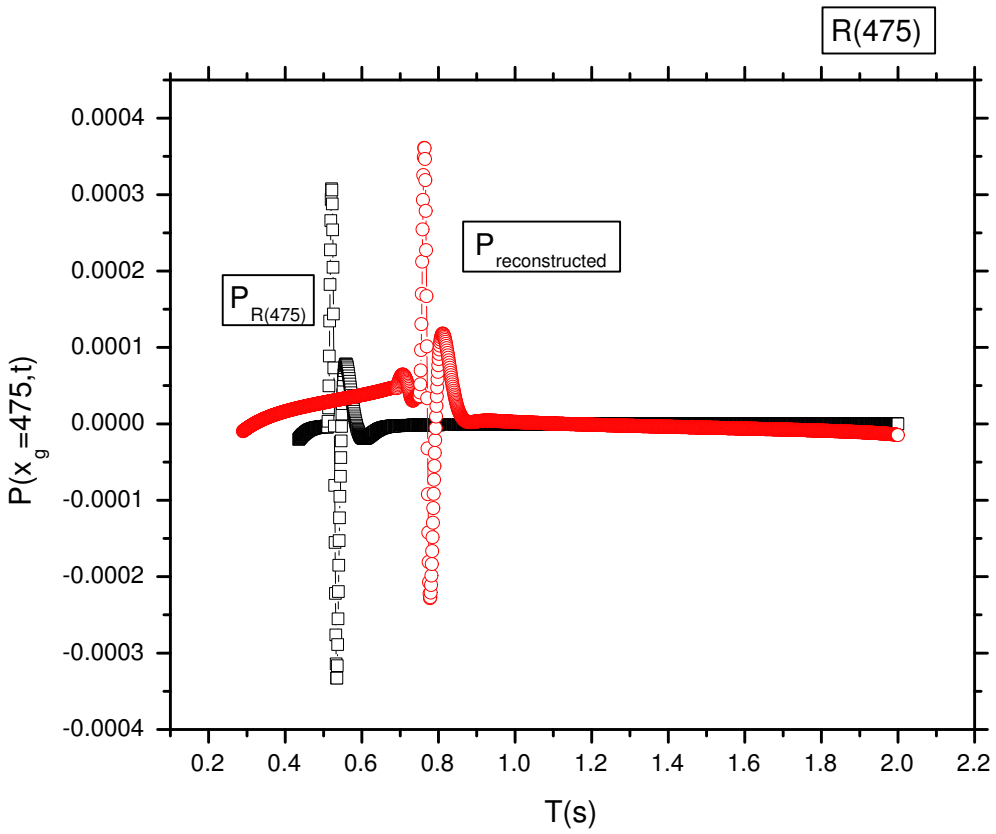

Figure 8*: Reconstructed and original data at 475 m from the source from a collection of data between offsets 900–1000 m in the post-critical zone and a separation of 5 m.*

surface multiples to new locations. The second order multiple it is also shown in Figure 15, there is no time delay between the reconstructed and the original one only under the consideration of extrapolating from pre-critical to pre-critical.

It appears that our algorithm properly reconstructs both primaries and multiples which is a necessary requirement for our objectives in multiple attenuation.

7 Contributions of the end points to the data reconstruction

If the aperture is compensated using a neutralizer function, there is an effect of the end points in the data reconstruction. As was shown previously, the migrated image (see Figure

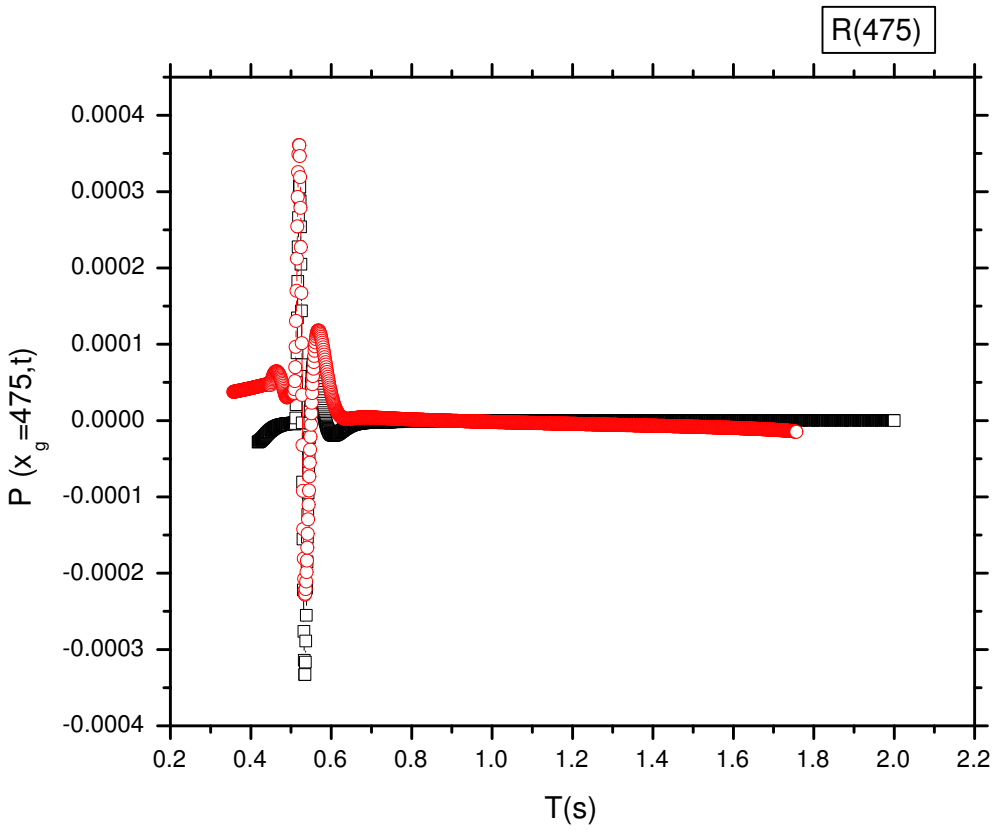

Figure 9*: Reconstructed and original data at 475 m from the source from a collection of data between 900–1000 m in the post-critical zone and a separation of 5 m shifted in time to make a comparison with the original data.*

4) is divided into three parts (37). The main contribution comes from the stationary point inside the aperture, followed by two terms coming from the end points.

To see how the end points contribute to the reconstruction of the data, we have reconstructed the data with and without contributions from the end points using the data with multiples. Figure 16 shows the reconstructed primary with and without the end point contribution. There is almost a perfect fit between the two traces which indicates that the end points is small in this specific example.

Figure 17 displays the reconstructed data for the first order multiple. As in Figure 16, we see no significant difference between the data reconstructed with and without the end point contribution. The comparison between the original data and the reconstructed with the contributions of the end points shows no improvement in amplitude.

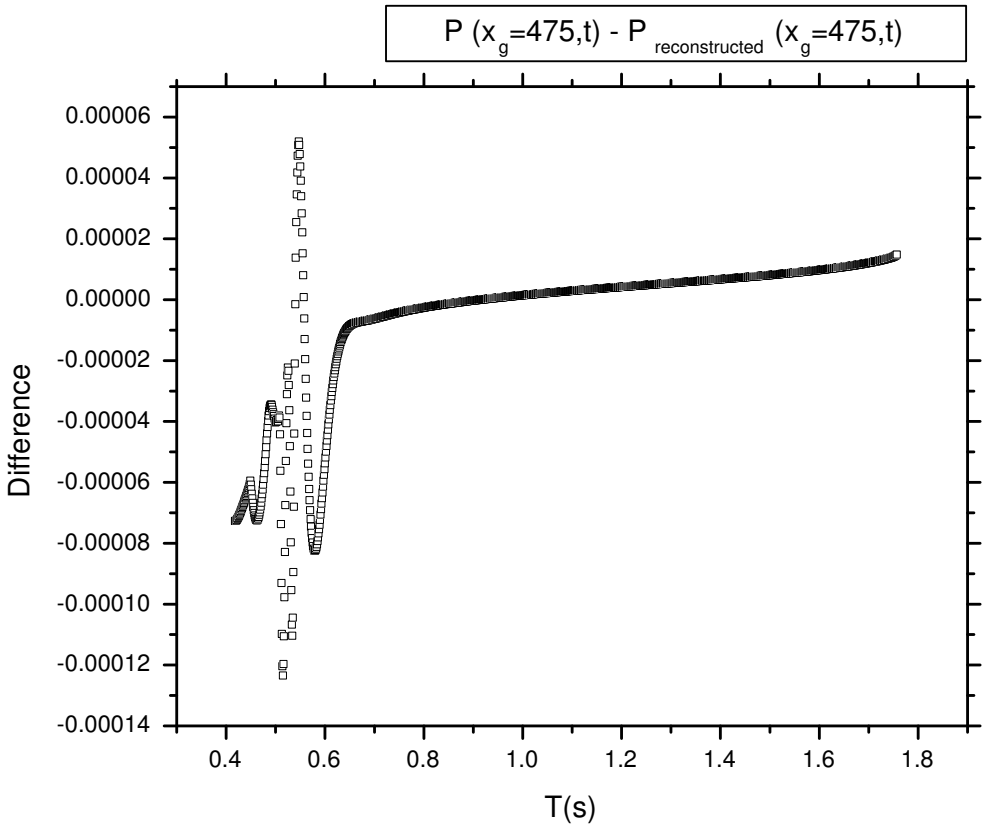

Figure 10*: Difference between the reconstructed data and actual data at 475 m from Figure 9. Notice the change in amplitude due to the presence of the head wave.*

8 Seismic data reconstruction for free surface multiple removal

There is recent interest in multiple attenuation technology resulting from current exploration challenges, e.g, in deep water with variable water bottom, in subsalt or shallow water exploration (Carvalho, 1992; Weglein et al., 2003).

These cases are representative of circumstances where 1-D assumptions are violated and subsurface information is not available. Inverse scattering multiple attenuation is designed to address these problems. It requires near source traces and other prerequisites. Motivated by this, we tested seismic data reconstruction with an eye to extrapolating traces for the inverse-scattering series multiple attenuation method.

The free surface demultiple algorithm (Weglein et al., 1997) can be summarized as follows:

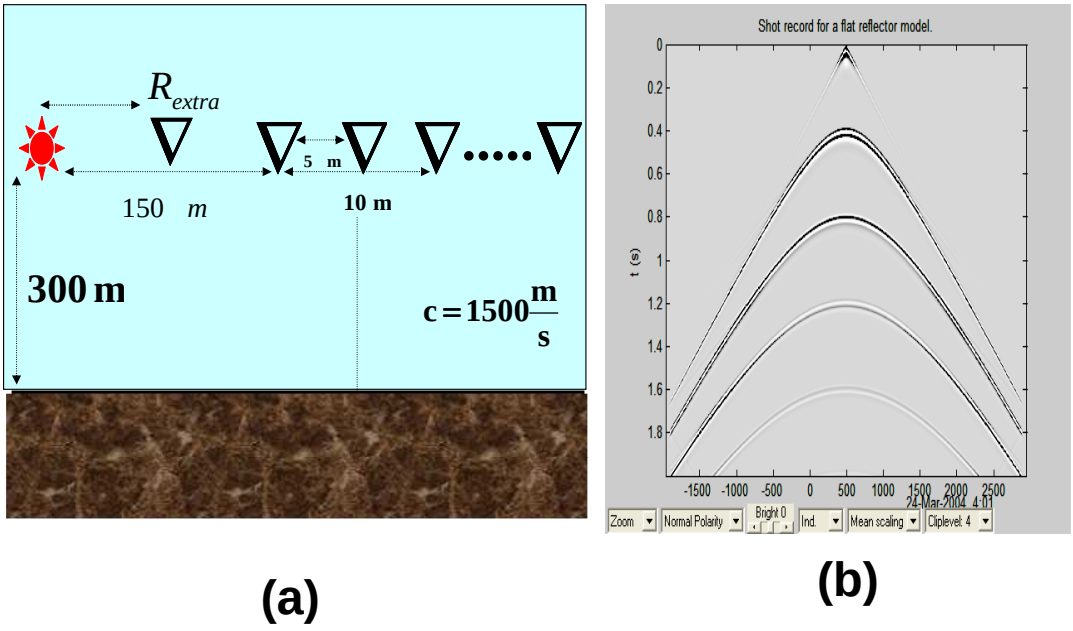

Figure 11: *(a) Schematic representation of the extrapolation experiment for a single interface model from pre-critical to pre-critical for a single interface with two medium velocities $c = 1500$ m/s and $v = 2250$ m/s and with a free surface at 15 m above the source and receivers. (b) Shot record of model (a) generated with finite differences.*

- The Data, D, are computed by subtracting the reference field, $G_0 = G_0^d + G_0^{FS}$ from the total field, G, on the measurement surface.
- Compute the deghosted data, $\tilde{D}$, where $\tilde{D} = D/[(e^{2iq_g\epsilon_g} - 1)(e^{2iq_s\epsilon_s} - 1)]$, ϵ_g, ϵ_s are source and receiver depths, and q_g, q_s are vertical wave numbers.
- For a 1D Earth $\tilde{D} = 2\pi\delta(k_g - k_s) \cdot \tilde{D}(k, \omega)$
- The series of deghosted and free-surface demultiple data, $\tilde{D}$, is given

$$D'(k, \omega) = \sum_{n=1}^{\infty} \tilde{D}_n(k, \omega) \tag{48}$$

where

$$\tilde{D}_n(k, \omega) = \frac{2q}{i\rho_r B(\omega)} \cdot e^{iq(\epsilon_g + \epsilon_s)} \cdot \tilde{D}_1(k, \omega)\tilde{D}_{n-1}(k, \omega). \tag{49}$$

We are going to generate one shot gather for a 1D Earth with a reflectivity code, see Figure 18, with a point source and receiver at a distance 30 m from the free surface.

We have a two layer model with 1500 m/s velocity in the first layer and 1800 m/s in the second layer. The minimum frequency is 10 Hz and the maximum is 80 Hz. The time sample rate is $dt = 0.001$ s, and the offset rate is $dx = 2$ m. We have taken into account a Q absorption value of 200 and constant density.

The first order free surface multiple can be seen in Figure 19. The next task is to evaluate seismic data reconstruction for a shot record with missing traces. Under this consideration we have used the original data from Figure 18 and eliminated some traces along the shot.

Using interpolation and extrapolation considerations we have been able to reconstruct the original data as it is shown in Figure 20b. Finally, this reconstructed data has been introduced as an input in the free surface demultiple algorithm. Figure **??** shows the results after removing multiples from this reconstructed data.

9 Conclusions

We have presented a procedure to interpolate and extrapolate traces to new locations from positions recorded. It consists of an integral operator considering the data in a continuous medium and is based on the assumptions that principle of superposition, physical invariance are satisfied. It also assume constant reference velocity and high frequency approximations.

The first test points out the crucial implication of what V_1 means. You can successfully interpolate traces and extrapolate from pre-critical to pre-critical and from post-critical to post-critical. The failure to extrapolate from post-critical to pre-critical in shows the intrinsic relation between the data and V_1. As mentioned earlier, the expression (9) is exact and precise without a thought or care about convergence, and it is the heart of the extrapolation scheme.

The first task, the inversion is performed via a stationary phase approximation. Under this consideration we have studied the implications to finite data, and we have calculated an aperture compensating factor. It was also shown that depending on the use of a neutralizer function or a taper function, the approximation breaks down because the integrand is not smooth. The contributions from the end points of the aperture need to be calculated to give validity to the stationary phase approximation.

The second task, demigration, has been accomplished using full wave theory, avoiding the same approximation that was made at the outset. We can summarize our results as follows:

- The reconstruction of seismic data can be done effectively in the pre-critical region.
- Extrapolating from post-critical to pre-critical confronts us with phase problems. There is a phase shift problem due to the reflectivity in the post-critical region.

- Corrected terms to the stationary phase approximation when we use a neutralizer function as an aperture compensator were calculated, but it doesn't improve the reconstructed amplitude.
- Seismic data reconstruction with free surface multiples for extrapolation near the source can be generated. Not only the primary reflection but also the first and second free surface multiples were estimated at the correct time using this extrapolation.
- Reconstructed data was presented from original data with missing traces, and the result of the reconstructed traces were shown.
- With the successful result of predicting the right time for the free surface multiple and the primary reflection we show the effect of the free surface removal on this reconstructed data.

Acknowledgements

We would like to thank the M-OSRP sponsors for making this work possible and for all the members of our team for their encouragement and support.

References

Bleistein, N. and R. Handelsman (1986). *Asymptotic expansions of integrals.* (2nd ed.). Dover Plub.Inc.

Carvalho, P. M. (1992). *Free-surface multiple reflection elimination method based on non-linear inversion of seismic data.* Ph. D. thesis, Universidade Federal da Bahia.

Claerbout, J. F. (1971). Toward a unified theory of reflector mapping. *Geophysics 36*(3), 467–481.

Hertweck, T. and A. Goertz (1999). On the aperture effects in 2.5-D kirchhoff migration. *SEGY 72*, 984–994.

Hubral, P., J. Schleicher, and M. Tygel (1996). A unified approach to 3d seismic reflection imaging part i. *Geophysics 61*, 742–758.

Jaramillo, H. and N. Bleistein (1997). Demigration and migration in isotropic inhomogeneuos medium. *SEG 63*, 1673–1676.

Santos, L., J. Schleicher, M. Tygel, and P. Hubral (2000). Seismic modeling by demigration. *Geophysics 65*, 1281–1289.

Stolt, R. H. (1978). Migration by Fourier transform. *Geophysics 43*(1), 23–48.

Stolt, R. H. (2002). Seismic data mapping and reconstruction. *Geophysics 67*, 890–908.

Stolt, R. H. and A. Benson (1986). *Seismic Migration* (2nd ed.). Geophysical Press.

Sun, J. (1998). On the limited aperture migration in two dimensions. *Geophysics 63*, 984–994.

Sun, J. (2002). Limited-aperture migration. *Geophysics 65*, 584–594.

Verschuur, D. J., A. J. Berkhout, and C. P. A. Wapenaar (1992). Adaptive surface-related multiple elimination. *Geophysics 57*, 1166–1177.

Weglein, A. B., F. V. Araújo, P. M. Carvalho, R. H. Stolt, K. H. Matson, R. T. Coates, D. Corrigan, D. J. Foster, S. A. Shaw, and H. Zhang (2003). Inverse scattering series and seismic exploration. *Inverse Problems 19*, R27–R83.

Weglein, A. B., F. A. Gasparotto, P. M. Carvalho, and R. H.Stolt (1997). An inverse-scattering series method for attenuating multiples in seismic reflection data. *Geophysics 62*, 1975–1989.

A Stationary phase approximation

Study of the contributions to the stationary phase approximation from the critical points depending on their location. Stationary point ξ_s near the end point $-\xi_a$:

$$I = I_s - I_{\xi_a} - I_{\xi_b} \tag{50}$$

$$I_{\xi_a} = H(-\epsilon) \cdot I_s + \epsilon \sqrt{\frac{2}{|\omega \tau^{"}(-\xi_a)|}} \times F_\gamma(u) G(-\xi_a)\, e^{i(\gamma u^2)} \tag{51}$$

$$\gamma = sgn(\omega \tau^{"}(-\xi_a)) \quad \epsilon = sgn(\xi_a + \xi_s) \quad u = |\tau^{'}(-\xi_a)| \sqrt{\frac{|\omega|}{|2\tau^{"}(-\xi_a)|}} \tag{52}$$

$$\sigma = sgn(\omega \tau^{"}(\xi_s)) \quad G(\xi) = E(\xi)\, e^{i\omega\tau(\xi_s)} \quad F_\sigma(\eta) \approx \frac{e^{i\sigma(\eta^2 + \pi/2)}}{2\eta}$$

$$I_{\xi_b} = -\frac{1}{i\omega} \frac{G(\xi_b)}{\tau'(\xi_b)} \tag{53}$$

$$I_s = \frac{\sqrt{2\pi}}{|\omega\tau"(\xi_s)|^{1/2}}\, G(\xi_s)\, e^{i\sigma\frac{\pi}{4}} \tag{54}$$

In the same way if we have the stationary point near the endpoint ξ_s near ξ_b:

$$I = I_s - I_{\xi_a} - I_{\xi_b} \tag{55}$$

$$I_{\xi_b} = H(-\epsilon)\cdot I_s + \epsilon\sqrt{\frac{2}{|\omega\tau"(\xi_b)|}} \times F_\gamma(u)\, G(\xi_b)\, e^{i(\gamma u^2)} \tag{56}$$

$$I_{\xi_a} = -\frac{1}{i\omega}\frac{G(\xi_a)}{\tau'(\xi_a)} \tag{57}$$

$$I_s = \frac{\sqrt{2\pi}}{|\omega\tau"(\xi_s)|^{1/2}}\, G(\xi_s)\, e^{i\sigma\frac{\pi}{4}} \tag{58}$$

In the situation of having the stationary point at the endpoint: $\xi_s = -\xi_a \Rightarrow I = \frac{I_s}{2} - I_{\xi_b}$ or in the case $\xi_s = \xi_b \Rightarrow I = \frac{I_s}{2} - I_{\xi_a}$.

When the stationary point is outside the migration aperture:

$$I = \frac{1}{i\omega}\left[\frac{G(\xi_b)}{\tau'(\xi_b)} - \frac{G(-\xi_a)}{\tau'(-\xi_a)}\right] \tag{59}$$

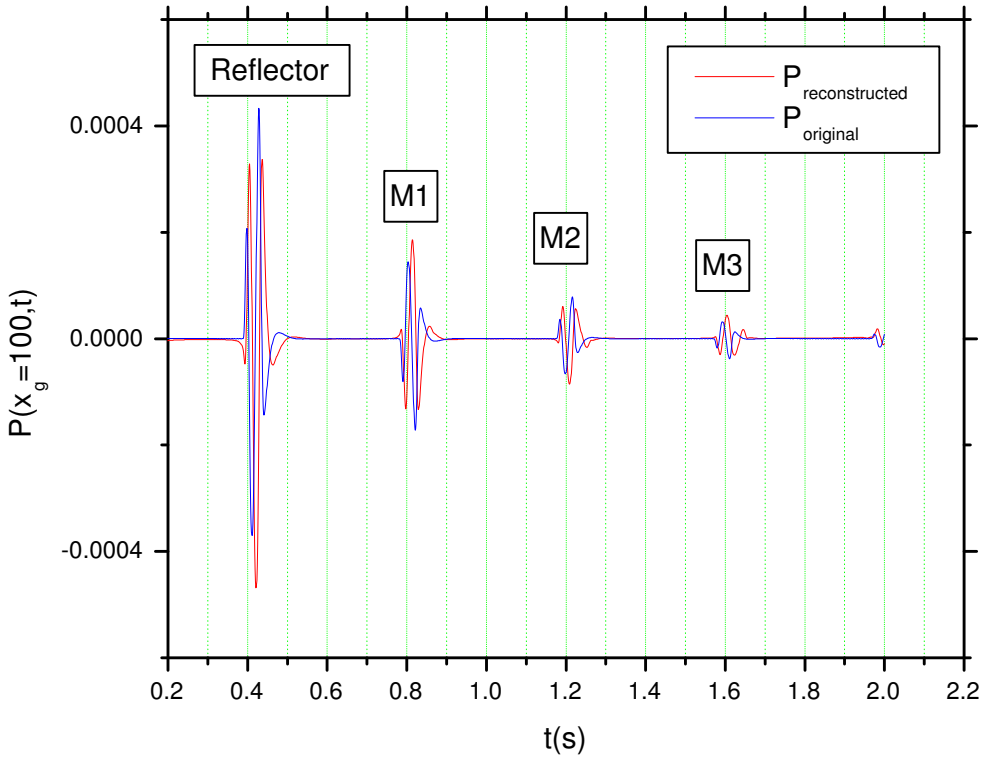

Figure 12*: Reconstructed and original data from the model in Figure 2 with the source and receivers 15 m below free surface extrapolated at 100 m from an offset range 150–500 m and a distance between receivers of 5 m.*

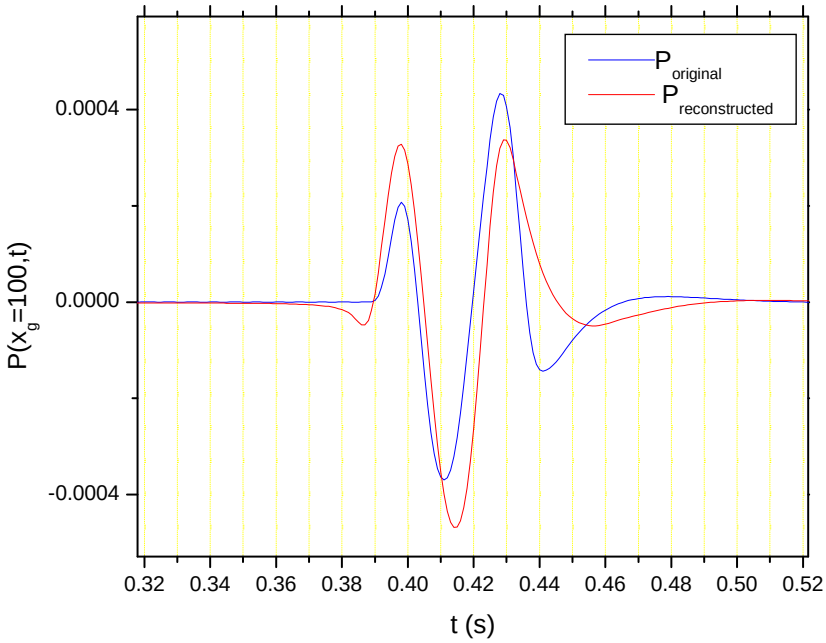

Figure 13*: Zoom of the primary reflection from Figure 12 where the original and reconstructed data are shown.*

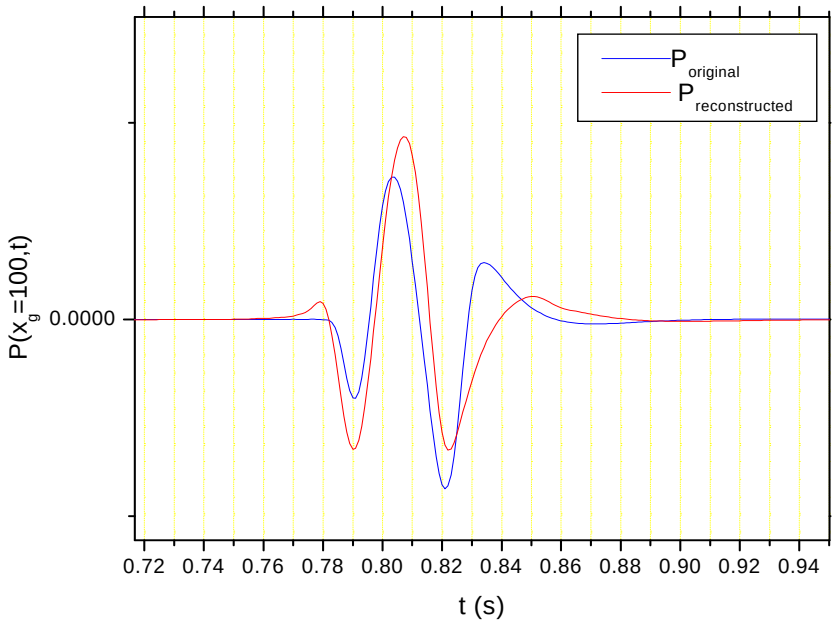

Figure 14*: Zoom of the first order free surface multiple from Figure 12 where the original and reconstructed data are shown.*

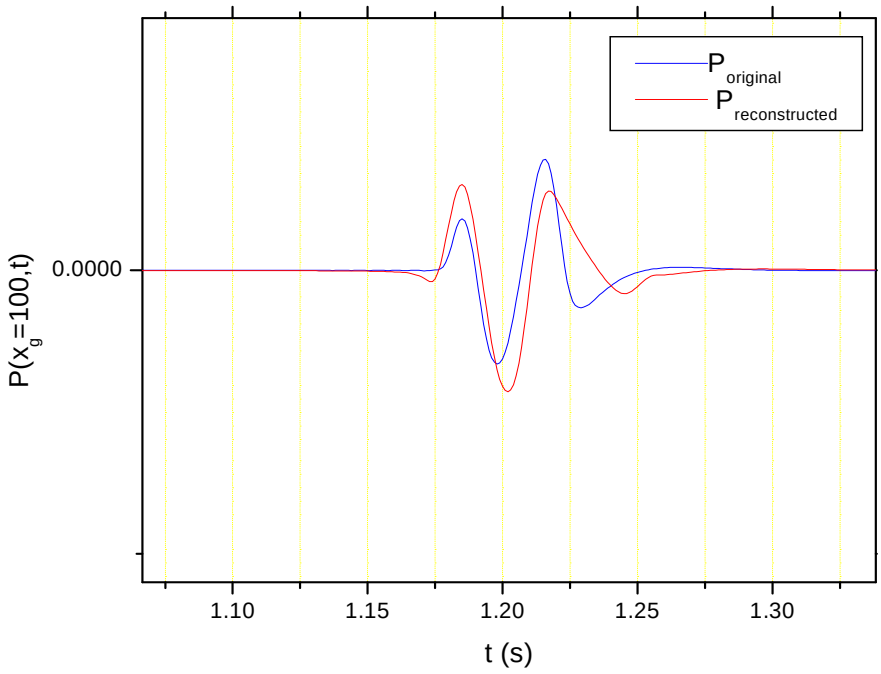

Figure 15*: Zoom of the second order free surface multiple from Figure 12 where the original and reconstructed data are shown.*

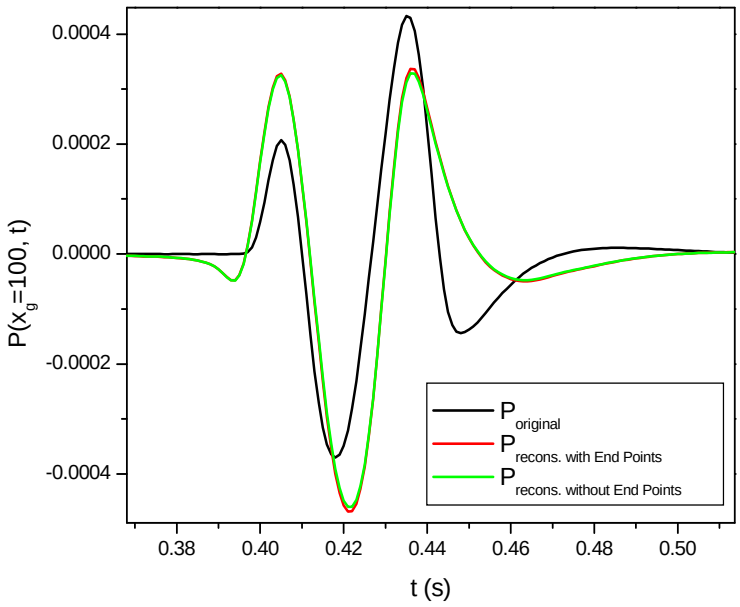

Figure 16*: Comparison of the primary reflection reconstructed with and without the end point contributions. As it is shown the contributions of the end points are small for this specific example. In general for dipping reflectors the influence can be estimated to be high.*

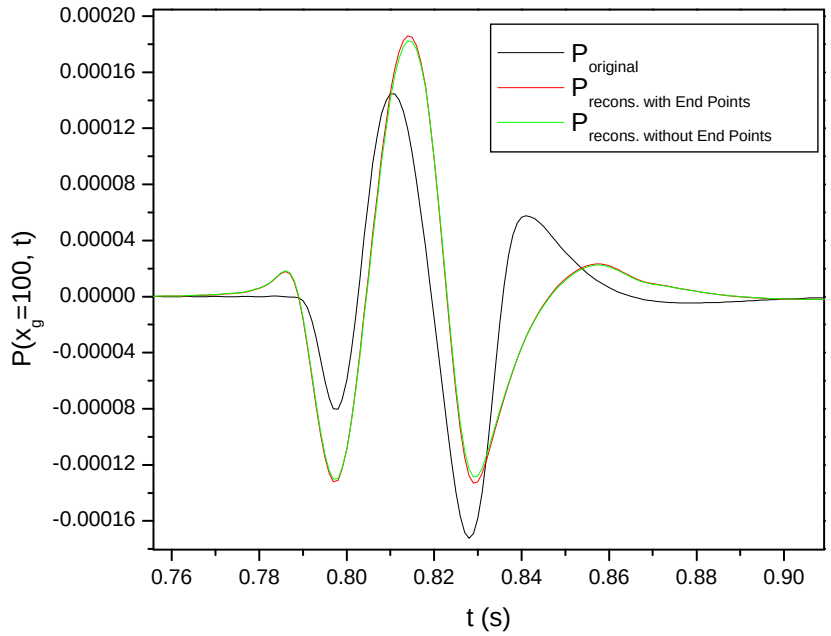

Figure 17*: Comparison of the first order free surface multiple reconstructed with and without the end point contributions. As it is shown the contributions of the end points are small for this specific example.*

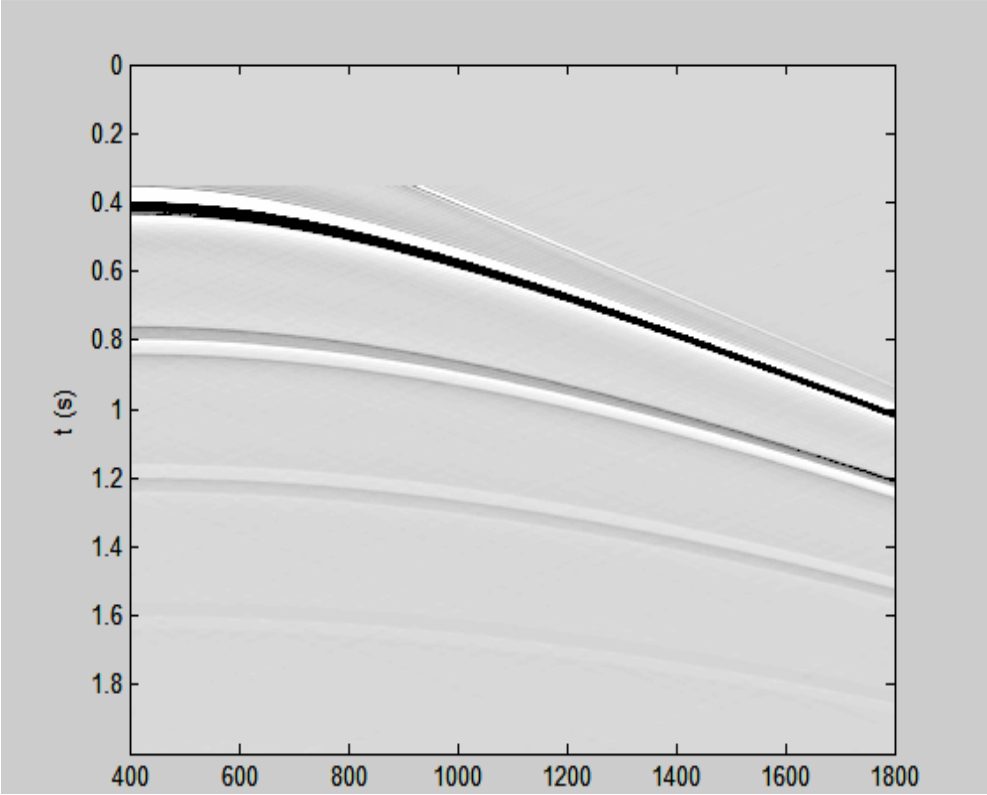

Figure 18*: Shot record gather with the source and receivers situated 30 m below free surface.*

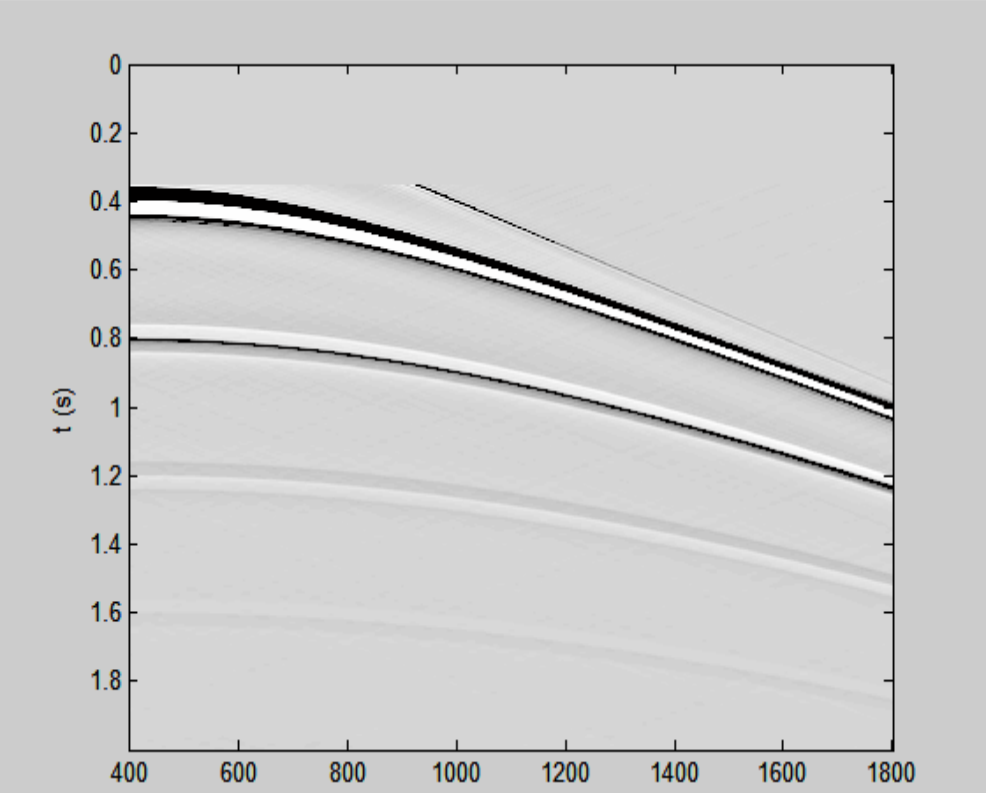

Figure 19*: Inverse polarity of Figure 18 to show the first order multiple we want to remove.*

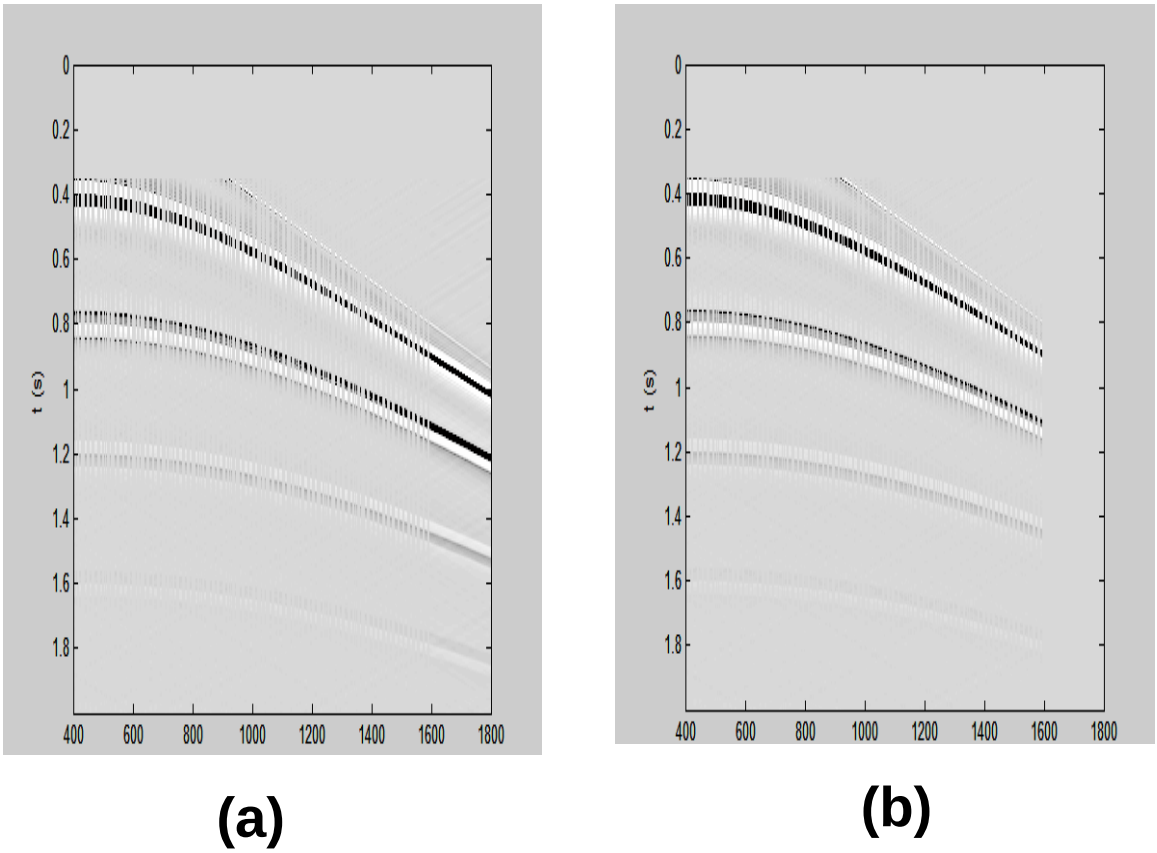

Figure 20*: Comparison of the original data with missing traces (a) and the reconstructed data (b).*

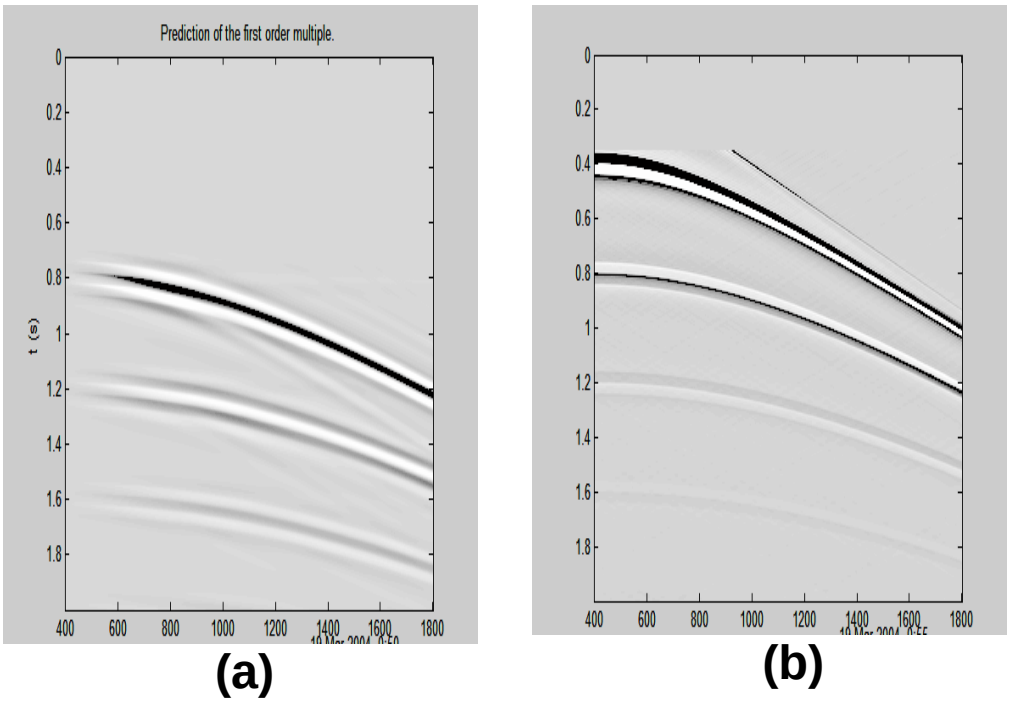

Figure 21*: Preliminary comparison of (b) the data from Figure 20 after data reconstruction with (a) the result of the free surface multiple prediction using the reconstructed data (displayed with inverse polarity to highlight the first order free surface multiple). The timing of the multiples has been well-predicted with the multiple prediction algorithm. The low amplitude on the near offsets of the prediction is due to the fact that the input data contained only positive offsets and no attempt was made to synthesize split-spread acquisition.*